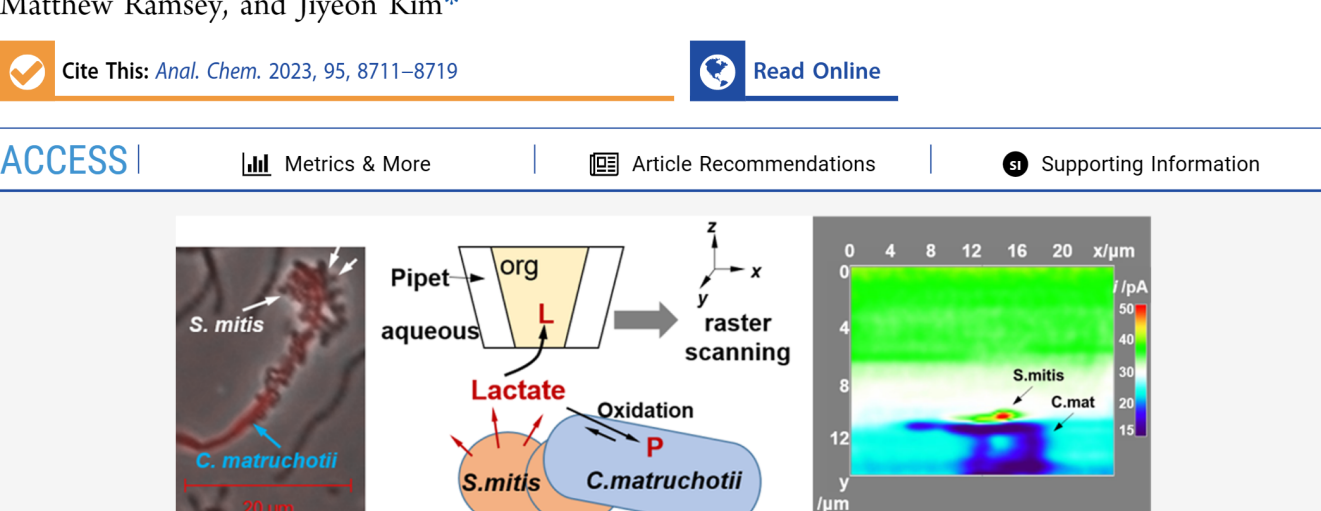


pubs.acs.org/ac Article

# Mechanistic Assessment of Metabolic Interaction between Single Oral Commensal Cells by Scanning Electrochemical Microscopy

Surendra R. Puri, Eric Almeida, Subhashini Elangovan, Alex Labossiere, Cybele Collins, Matthew Ramsey, and Jiyeon Kim\*



ABSTRACT: The human oral microbiome heavily influences the status of oral and systemic diseases through different microbial compositions and complex signaling between microbes. Recent evidence suggests that investigation of interactions between oral microbes can be utilized to understand how stable communities are maintained and how they may preserve health. Herein, we investigate two highly abundant species in the human supragingival plaque, *Streptococcus mitis* and *Corynebacterium matruchotii*, to elucidate their real-time chemical communication in commensal harmony. Specifically, we apply nanoscale scanning electrochemical microscopy (SECM) using a submicropipet-supported interface between two immiscible electrolyte solutions as an SECM probe not only to image the permeability of *S. mitis* and *C. matruchotii* membranes to tetraethylammonium (TEA<sup>+</sup>) probe ions but also to real-time visualize the metabolic interaction between two microbes via lactate production/consumption at a single-cell level. The metabolic relationship between two strains is quantitatively assessed by determining (1) the passive permeability of both bacterial membranes of 2.4 × 10<sup>-4</sup> cm/s to the free diffusion of TEA<sup>+</sup>, (2) 0.5 mM of the lactate concentration produced by a single *S. mitis* strain at a rate of 2.7 × 10<sup>-4</sup> cm/s, and (3) a lactate oxidation rate ≥5.0 × 10<sup>6</sup> s<sup>-1</sup> by an individual *C. matruchotii* strain. Significantly, this study, for the first time, describes a mechanism of in situ metabolic interaction between oral commensals at the single-cell level through quantitative analysis, which supports the observed in vivo spatial arrangements of these microbes.

## **■ INTRODUCTION**

Among various human habitats, the oral cavity retains a rich and complex ecosystem accommodating different microbes, i.e., the oral microbiome<sup>1</sup> that thrive in the dynamic oral environment in a symbiotic relationship with the human host.<sup>2</sup> The unique microbial composition, however, is significantly affected by interspecies and host—microbial interactions, which can subsequently impact the health and disease status of the host.<sup>3,4</sup> Moreover, the destruction of the oral microbial community is related to systemic diseases such as cancers, cardiovascular diseases, Alzheimer's disease, and diabetes.<sup>1,5,6</sup> Accordingly, mechanistic interaction data between species are urgently needed to understand how changes in oral microbiome composition precede clinical signs of disease, thereby preventing the development of disease while preserving the health of the community.

Regardless of health status, a robust polymicrobial biofilm has been found in supragingival plaque (SUPP), where two highly abundant species, *Corynebacterium matruchotii* and *Streptococcus mitis*, coexist. Recent microscopy studies discovered the unique spatial organization between these two species forming a "corncob" structure in vivo, where the long filamentous *C. matruchotii* is surrounded by *S. mitis*. his distinctive morphology is ascribed to *C. matruchotii*'s role in tethering and bridging colonizers, e.g., *S. mitis* within plaque. *S. mitis* are Gram-positive oral microbes that ferment glucose to lactate and produce hydrogen peroxide under aerobic conditions. The production of H<sub>2</sub>O<sub>2</sub> enables beneficial oral

**Received:** April 6, 2023 **Accepted:** May 11, 2023 **Published:** May 25, 2023





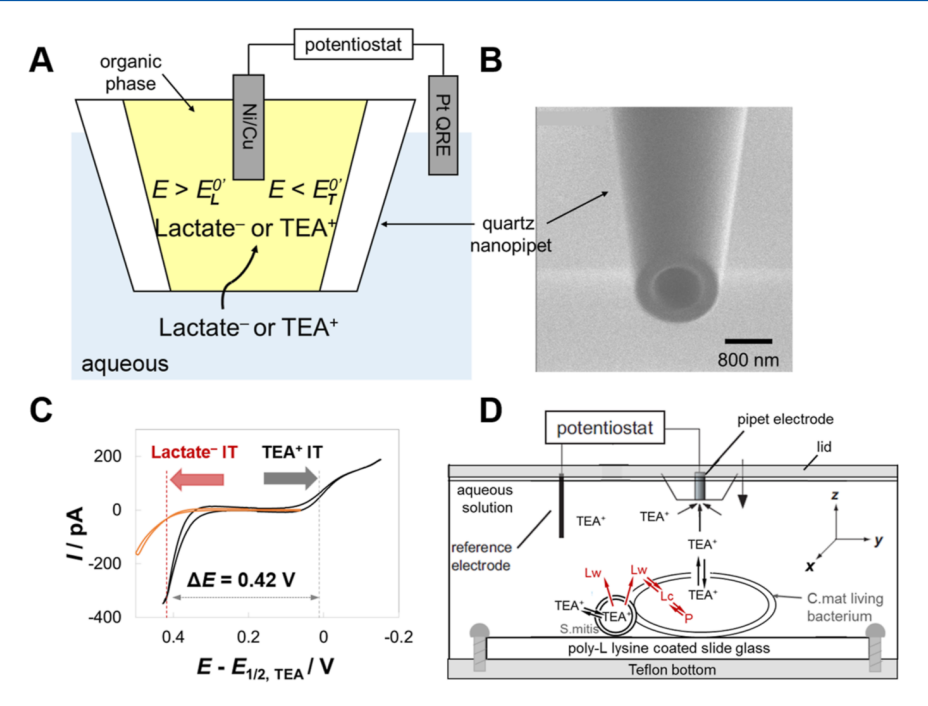


Figure 1. (A) Illustrated scheme of a submicropipet-supported ITIES to directly probe  $TEA^+$  IT or lactate IT, (B) SEM image of a pipet tip, (C) cyclic voltammograms of  $TEA^+$  and lactate ITs in buffer solution containing 1 mM  $TEA^+$  and 2 mM lactate (a background voltammogram obtained in buffer solution in yellow solid line, scan rate = 25 mV/s), (D) schematic of the SECM setup with living coculture bacteria immobilized on poly-L-lysine-coated slide glass, where constant-height SECM imaging or SECM approach curve is measured over *S. mitis* and *C. matruchotii* coculture using a pipet tip, respectively.

streptococci to compete in the oral environment and can be a source of stress upon adjacent species. <sup>12</sup> In a parallel study, we have identified how *C. matruchotii* responds to *S. mitis* H<sub>2</sub>O<sub>2</sub>-dependent stress as well as lactate production. <sup>13</sup> While the spatial organization/biogeography of these species has been well described, the exact nature of molecular interactions between these species, especially between individual cells, is relatively unknown. Accordingly, we seek to study these metabolic interactions by directly probing local metabolites, i.e., pristine lactate near individual bacteria to gain mechanistic insights into how these interactions contribute to in vivo association.

Herein, we employ nanoscale scanning electrochemical microscopy (NanoSECM) to determine the mechanistic understanding of metabolic cooperation between commensal bacteria at a single-cell level. Recently, SECM has been applied to study metabolic interactions in various microbial systems, including biofilms and small aggregates, owing to its unique capability of studying real-time metabolic exchange between relevant species in a controlled spatial proximity. <sup>14–19</sup> In fact, real-time SECM imaging of interspecies biofilms or aggregates not only quantified the local concentration of metabolites but also visually confirmed metabolic cross-talk between species. 14-17 However, a few or tens of micrometer-sized probes with the corresponding instrumentation provide limited spatial and temporal resolutions, thus remaining a major challenge in grasping detailed mechanistic perceptions. In contrast, Nano-SECM features precise tip-positioning capability at nanometer scale and nanometer-sized probes offering high spatial resolution at the nanometer scale and rapid temporal resolution at the micro-second scale. 20–22 Therefore, Nano-SECM is suitable for studying a single bacterium and mapping/quantifying the local concentration of metabolites produced or consumed in situ between single bacterial cells,

thereby revealing/quantitatively assessing the mechanistic interaction between species at single-cell resolution in real time

In this work, we investigated two highly abundant species in the human SUPP, S. mitis and C. matruchotii, to elucidate their real-time chemical communication approximating their healthy commensal status. We resolved each single cell of C. matruchotii and S. mitis in coculture and performed in situ and real-time imaging of the metabolic interactions between these species as well as of the topography of single cells by employing SECM tips based on submicro-pipet-supported interfaces between two immiscible electrolyte solutions (ITIES) (Figure 1A). With this pipet tip, a Ni/Cu electrode in the internal organic electrolyte applied a potential bias across the liquid/liquid interface with respect to a Pt quasi reference electrode in the aqueous solution to yield the amperometric tip current based on the selective interfacial transfer of a small probe ion, tetraethyl ammonium (TEA+) ion, or a small metabolite ion, i.e., lactate-. Measurements of the SECM approach curve and the real-time SECM imaging of coculture based on TEA+ ion transfer (IT) allowed us to determine the intrinsic permeability of both bacterial membranes (BMs) and topography of bacteria, respectively. Subsequently, SECM imaging based on lactate IT was studied to map the local concentration of lactate near individual S. mitis and C. matruchotii in coculture, and probe their metabolic interaction via metabolic exchange, i.e., in situ production and consumption of lactate, respectively. Importantly, the quantitative analysis of SECM data using finite element simulations provides mechanistic assessment of the metabolic interactions between commensal bacteria at a single-cell level, where the level of lactate concentration produced by a single *S*. mitis strain, the lactate production rate at a single S. mitis cell level, and the consumption rate of lactate by a single C.

matruchotii strain could be defined for the first time. This study provides additional key insights into the in vivo spatial arrangements and co-occurrence between two commensals in healthy oral biofilms, as studied by optical and fluorescence microscopy.<sup>23</sup>

## **■ EXPERIMENTAL SECTION**

**Strains and Media.** *C. matruchotii* (ATCC 14266) and *S. mitis* (ATCC 49456) were grown on brain heart infusion media supplemented with 0.5% yeast extract (BHI-YE) at 37  $^{\circ}$ C in a static incubator with 5% CO<sub>2</sub> or in 5% H<sub>2</sub>, 10% CO<sub>2</sub>, and 85% N<sub>2</sub> under anaerobic conditions. More details about growth of coculture and monoculture are explained in the Supporting Information.

SECM Sample Preparation. Bacteria were grown overnight in BHI-YE and then washed by centrifugation in a defined medium, which is an amended version of Teknova EZ RICH (Teknova, M2105). The medium was prepared as described in the manufacturer's instructions with the addition of vitamin solution, lipoic acid, folic acid, riboflavin, NAD+, and nucleotides at final concentrations from that of a chemically defined medium previously described 13 and glucose at 10 mM. Bacteria were grown to an OD<sub>600</sub> of 0.3-0.5 and then diluted to final concentrations of  $1.2 \times 10^7$  and  $6.0 \times 10^6$ cfu of C. matruchotii and S. mitis, respectively, in 200 µL of defined medium. This was then incubated at 37 °C with 5%  $CO_2$  for 1 h. 10  $\mu$ L of this solution was then added to a polylysine-coated glass slide and incubated at 37 °C for 15 min after which medium was removed by a micropipette to remove planktonic cells and ensure that only attached cells remained. An additional 10  $\mu$ L of pre-warmed defined medium was then added to a poly-L-lysine-coated glass slide (Glass Microscope Slides Rite-On) of 15 mm  $\times$  9 mm size. The glass slide was rinsed by buffer media to remove loosely bound bacteria on the glass surface and then assembled in SECM cell for further analysis.

1 mM tetraethylammonium chloride (TEA<sup>+</sup>Cl<sup>-</sup>, Sigma-Aldrich) solution was prepared in freshly prepared oral bacterial growth media at  $\sim$ pH 7.5, where TEA<sup>+</sup> was used as a probe ion. The solution was then filtered with a syringe filter (0.1  $\mu$ m filter unit, SLVV033RS, Duropore PVDF membrane, MILLEX VV) and further filled the SECM cell containing a bacterial sample. TEA<sup>+</sup> is particularly chosen, which does not affect the growth rate of each bacterial cell, thus maintaining the same physiological activity (data not shown).

Fabrication of Submicro-Pipet Electrodes as SECM Tips. Fabrication of sub-microsized pipet electrodes has been reported elsewhere.<sup>24</sup> Briefly, a quartz capillary (outer diameter 1 mm, inner diameter 0.7 mm, length 10 cm, Sutter instrument) was cleaned by blowing with compressed air, and pulled with a CO<sub>2</sub> laser puller (model P 2000-2035, Sutter Instrument) (parameters: heat = 720, filament = 4, velocity = 30, delay = 130 and pull = 110) with a ca. 800 nm inner diameter. As-pulled pipets were cleaned by a UV plasma cleaner (PDC-32G, Harrick Plasma). Further, the cleaned pipets were silanized by the chemical vapor deposition method using 50 µL of N,N-dimethyltrimethylsilylamine inside the vacuumed desiccator for 50 min under a constant relative humidity of 16% at 20 °C. The resulting silanized pipets were then filled with 10  $\mu$ L of 1,2-dichloroethane containing 0.1 M tetrakis(pentafluorophenyl) borate-tetradodecylammonium+ (TFPB-TDDA+) as supporting electrolytes.<sup>24</sup> An electrochemically etched Ni/Cu wire was inserted inside a pipet as an inner reference electrode and was immobilized for electrochemical measurements. Potential was applied between a submicropipet tip (a Ni/Cu inner reference electrode) and a Pt quasi reference electrode by a potentiostat (CHI 8022D, CH Instruments, TX, Austin) during SECM measurements.

Article

Nanoscale SECM Measurements. A home-built nanoscale scanning electrochemical microscope equipped with an isothermal chamber is employed to measure approach curves and image single bacterial cells at ~32 °C. In bulk solution containing TEA+, cyclic voltammetry was performed to estimate a steady state current of a pipet tip  $(i_{T,\infty})$  for electrochemical characterization (eq 1). Then, the pipet tip was vertically approached over a glass substrate by SECM until it showed a sharp decrease in current, i.e., feedback current response. Once we observed a foot of feedback current, the pipet tip was withdrawn 6  $\mu$ m above, and approached at a slow rate of 10 nm/s (1 nm step size/100 ms incremental time) until tip currents decreased to ca. 93-90% of  $i_{T,\infty}$ , corresponding to a distance from the substrate equivalent to a tip diameter. Subsequently, a tip was further withdrawn ~2  $\mu$ m to prevent a tip crash with possible clumps of bacteria in coculture or monoculture during raster scanning. SECM imaging was performed at constant height mode. For SECM imaging, a pipet tip monitoring TEA+ IT was raster scanned along the x- and y-axes at 1  $\mu$ m/s (i.e., 100 nm step size/100 ms incremental time) in the 25  $\mu$ m × 25  $\mu$ m region to obtain a topographical image of the bacterial cells. Then, a pipet tip was brought to the original starting point. The pipet tip potential was switched to a potential to sense lactate IT (~0.42 V more positive than  $E_{1/2}$  of TEA<sup>+</sup> IT, as shown in Figure 1C). The tip was continuously raster scanned in the same 25  $\mu$ m  $\times$  25  $\mu$ m region to real-time monitor the lactate production/consumption by bacteria in situ. The permeability of the BM was studied by measuring SECM approach curves over the center of a bacterial cell. Numerical simulations using finite element methods with COMSOL Multiphysics are explained in the Supporting Information.

# ■ RESULTS AND DISCUSSION

Electrochemical Sensing of Probe lons, TEA+ and Metabolite lons, Lactate -. We employed a submicropipetsupported ITIES as a probe<sup>24</sup> to in situ investigate the topography of bacteria and real-time map the metabolites, i.e., lactate surrounding an individual bacterium. With this pipet tip filled with an electrolyte solution of 1,2-dichloroethane (DCE), an amperometric tip current is selectively monitored based on interfacial ITs of TEA+ as a probe ion, or lactate as a metabolite produced or consumed by bacteria, respectively (Figure 1A,B). Herein, TEA+ IT is monitored at a negative potential to study the topography of bacteria without affecting their physiological activity, while lactate is sensed at a positive potential to in situ monitor the chemical interaction between bacteria (Figure 1C). A coculture of C. matruchotii and S. mitis at a low optical density (OD 0.3-0.5) is immobilized over a poly-L-lysine-coated slide glass plate and studied by raster scanning or vertically approaching a ~400 nm inner radius tip over individual bacteria (Figure 1D). Under negative potential applied to a tip, the current for TEA+ IT is lowered as the tip moves laterally toward the bacteria with a submicrometer gap between the tip and a bacterium, where bacteria hinder the diffusion of TEA+ to the tip. Subsequently, the tip current is recovered over the glass substrate, thereby yielding topographical information of the bacterial sample. After the tip

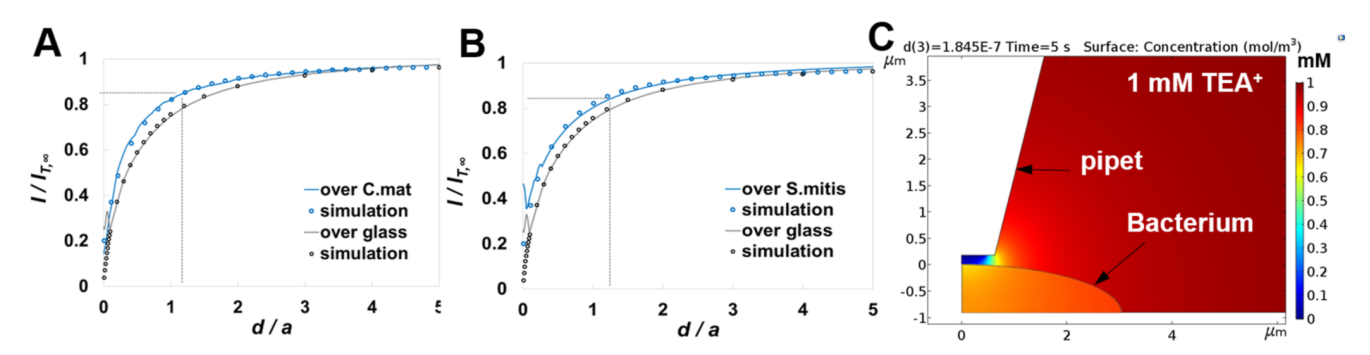


Figure 2. SECM approach curves based on TEA<sup>+</sup> IT (A) over *C. matruchotii* (blue solid curves) and (B) over *S. mitis* (blue solid curves). Both curves are overlaid with a curve over an insulating glass substrate (gray solid curves). Experimental curves (blue solid curves) are compared with theoretically simulated ones (blue open circles) with permeability,  $k_1 = 2.4 \ (\pm 0.1) \times 10^{-4} \ cm/s$ . Theoretically simulated negative feedback approach curves are shown as black open circles. (C) Concentration profile of TEA<sup>+</sup> ions near *C. matruchotii* and a pipet tip.

potential is switched to more positive than TEA+ IT (0.41-0.42 V more positive than  $E_{1/2}$  of TEA<sup>+</sup> IT) and induces lactate IT, the tip scans the same region as topography study to directly sense lactate near bacteria, thus mapping the local lactate as a result of in situ metabolic activity. Notably, a tip with 400 nm inner radius is sufficiently small to spatially resolve each single bacterium and real-time probe the chemical interactions between bacteria at a single-cell level, as S. mitis is characteristically round-to-ovoid coccus with 0.6-1.0 µm in diameter,  $^{25}$  and C. matruchotii is ca. 0.8  $\mu$ m in diameter and 1.5-8.0  $\mu$ m in length.<sup>26</sup> In fact, even smaller tips could enhance the spatial resolution in the SECM measurements. Irregular and various sizes of bacteria in coculture, however, readily induce tip crashes during raster scanning a small tip within a nanometer gap above bacteria. Accordingly, a ~400 nm radius tip was chosen to avoid tip crashes without compromising spatial resolution in our SECM study.

Determination of BM Permeability to Passive Diffusion of TEA<sup>+</sup> Studied by SECM and Finite Element Simulation. The inherently low permeability of the Grampositive BM was investigated by vertically approaching a tip above a single bacterium with SECM, where tip currents were monitored by varying the distance between a tip and BM, a.k.a. an SECM approach curve. SECM approach curves were measured right above *S. mitis* and *C. matruchotii*, respectively, to characterize the passive permeability of each BM to a probe ion, TEA<sup>+</sup>. When the tip was positioned far from the BM, the stable amperometric current based on the diffusion-limited IT of TEA<sup>+</sup> was obtained, as shown below.<sup>24</sup>

$$i_{\mathrm{T},\infty} = 4\delta z F D_{\mathrm{w}} c^* a \tag{1}$$

where  $i_{\rm T,\infty}$  is a current in bulk,  $\delta$  is the function of RG ratio (RG is the ratio of the outer and inner diameters of a glass pipet,  $\delta=1.16$  for a RG 1.5 tip), z is a charge of TEA<sup>+</sup>, F is the Faraday constant (96,485 C/mol),  $D_{\rm w}$  is the diffusion coefficient (6 × 10<sup>-6</sup> cm<sup>2</sup>/s),  $c^*$  is a bulk concentration of TEA<sup>+</sup> (1.0 mM), and a is the inner radius of a pipet tip (430 nm). The tip radius was estimated from  $i_{\rm T,\infty}$  and RG value determined by the SEM image (Figure 1B).

Well-defined approach curves were obtained for both C. matruchotii and S. mitis (Figure 2A,B, respectively). The tip current,  $i_T$ , began decreasing significantly  $\sim 2.0~\mu m$  above BMs because the nonspecific diffusional flux of TEA<sup>+</sup> induced by its IT at the tip was mediated only through porin-channels and was blocked by the rest of the lipid bilayer membrane. In Figure 2, SECM approach curves are constructed by

normalizing tip displacements (d) with respect to the tip inner radius (a), i.e., d/a, where the zero in d/a denotes zero distance between the BM and the tip (blue solid curves in Figure 2A,B). SECM approach curves over a flat, smooth, and insulating glass substrate were separately measured, which show a decrease in currents over a glass substrate due to the hindered diffusion of TEA<sup>+</sup> to the tip, i.e., negative feedback effect, and a sharp spike at  $\sim$ 30 nm above a glass substrate corresponding to a contact between a glass substrate and a glass sheath surrounding a tip (gray solid curves in Figure 2A,B). SECM approach curves measured over a bacterium are overlaid with negative feedback approach curves to consistently set the contact point between the BM and the tip. Importantly, the close contact distance is required to minimize the uncertainty in determining the permeability of the BMs.

The low permeability of both *S. mitis* and *C. matruchotii* BMs to TEA<sup>+</sup> was determined by fitting the experimental approach curves with the theoretical curves obtained by the finite element simulation of a two-phase SECM diffusion problem. The tip current was calculated from the concentration profile of TEA<sup>+</sup> in 2D simulation at various tip–BM distances, d (Figure 2C). In this simulation, the BM was treated as a homogeneous membrane with inherent permeability,  $k_1$ , as given by

$$TEA^{+}$$
 (outer solution)  $\underset{k_{2}}{\rightleftharpoons}$   $TEA^{+}$  (inside bacterial cell) (2)

where the permeability of  $k_1$  and  $k_2$  for passive influx and efflux of TEA<sup>+</sup>, respectively, corresponds to the equilibrium concentration of TEA<sup>+</sup> in the bulk outer solution and the bacterium. The equilibrium concentrations of small probe ions in the outer solution and in the bacteria,  $c_1^0$  and  $c_2^0$ , respectively are related to the partitioning equilibrium constant,  $K_e$ , and assumed to be  $\sim 0.9$  for monovalent ion<sup>27</sup>

$$K_{\rm e} = \frac{c_2^0}{c_1^0} = \frac{k_1}{k_2} \tag{3}$$

Since small and hydrophilic TEA<sup>+</sup> ions freely diffuse through porins, <sup>28</sup> a kinetic effect on an approach curve results from the impermeable region of the BM. This kinetic effect can be seen in the discontinuous concentration profile of TEA<sup>+</sup> across the BM under the tip (Figure 2C).

Experimental approach curves agreed well with simulated ones to yield a passive BM permeability,  $k_1$  of 2.4(±0.1) ×  $10^{-4}$  cm/s, identical for both *C. matruchotii* and *S. mitis* (Figure

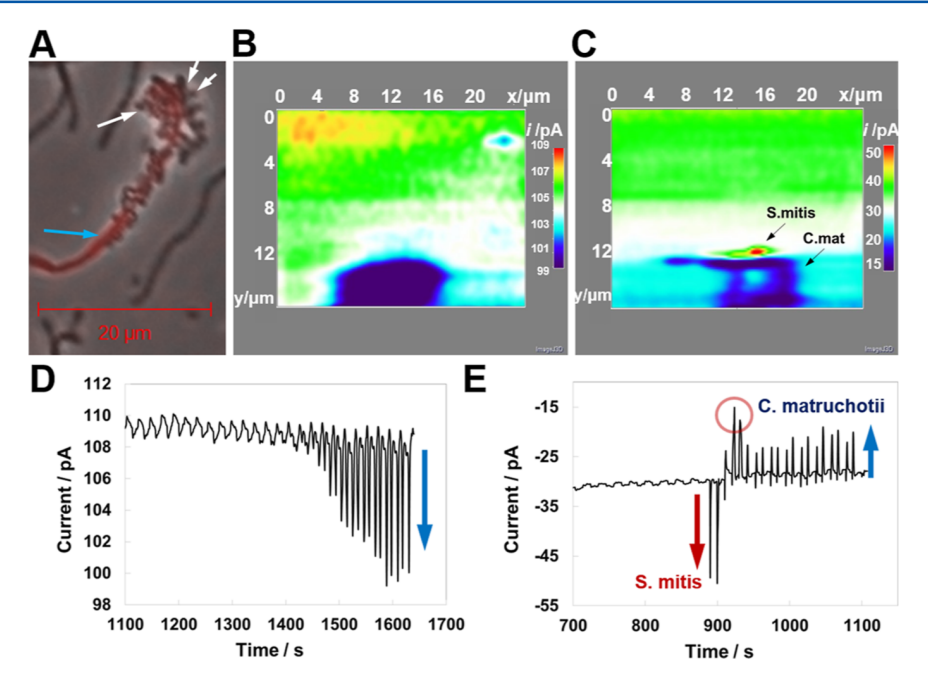


Figure 3. (A) Optical microscopic image of *C. matruchotii* (blue arrow) and *S. mitis* (white arrows) coculture. Constant-height SECM images based on (B) TEA<sup>+</sup> IT (obtained with a gap between the tip and bacteria of 1.75 d/a) and (C) lactate IT (obtained at the gap of 1.20 d/a), tip scan rate during SECM imaging at 100 nm/100 ms. Chronoamperometric responses based on (D) TEA<sup>+</sup> IT and (E) lactate IT (raw data, cross-sections of SECM images in (B) and (C), respectively). The current polarity is set to positive for cationic current responses (D) and negative for anionic current responses (E).

2A,B, blue open circles, see the Supporting Information). The numerical analysis confirms that the contact of the tip with the BM occurred at 30-40 nm. This nanoscale contact distance is critical to unequivocally resolve the approach curves as obtained over bacteria and over a glass substrate.<sup>29</sup> In this distance range, the tip current decreased rapidly and distinctly as the tip approached the BM. Noticeably, the BM permeability determined from the approach curves contains an uncertainty of less than 5% owing to the short non-zero distances at the tip-BM contact. Also, a mass transfer coefficient at this nanogap (d = 30 nm), i.e.,  $D_w/d$  of ~2.0 cm/s across the tip-BM gap was 4 orders of magnitude higher than the  $k_1$  values, thereby confirming the reliability of the determined permeability values. Notably, the determined permeability of Gram-positive BMs is 10-100-fold lower than other biological membranes such as algal protoplast cell membranes and the nuclear envelope. 27,29 Herein, TEA<sup>+</sup> was used in lieu of lactate to determine BM permeability for two reasons, i.e., the same charge amount  $(\pm 1)$  and similar diffusion coefficients of  $\sim 6 \times 10^{-6}$  cm<sup>2</sup>/s in water.

Real-Time Electrochemical Mapping of Local Lactate Reveals In Situ Metabolic Interaction between *S. mitis* and *C. matruchotii* via Simultaneous Lactate Production and Consumption. To image the coculture of *S. mitis* and *C. matruchotii* for topography and metabolic activity (Figure 3A), the constant-height mode of nanoscale SECM was employed. The submicro-tip enabled us to obtain SECM images with a high spatial resolution to resolve the pristine living coculture of *S. mitis* and *C. matruchotii* immobilized on poly-lysine-coated glass. For the topographical study, a tip monitoring TEA<sup>+</sup> IT approached vertically with the gap between the tip and bacteria,  $d = 0.75 \ \mu\text{m}$ , i.e.,  $1.75 \ d/a$  with the tip radius,  $a = 430 \ \text{nm}$ , then raster scanned for constant-height image of coculture. Low tip currents of ~89% of  $i_{T,\infty}$  above bacteria were obtained due to hindered diffusion of

TEA<sup>+</sup> by bacteria with merely permeable membrane to TEA<sup>+</sup> (Figure 3B). In fact, individual bacteria tangled with each other could not be differentiated in this topographical SECM image, and a lump appeared in the 25  $\mu$ m × 16  $\mu$ m image. As shown in the chronoamperometric responses, i.e., cross sections of the SECM image in Figure 3B, currents were monotonically decreasing in 1450–1650 s (positive polarity for cationic currents) due to the hindered diffusion of TEA<sup>+</sup> to the tip right above bacteria (shown as raw data in Figure 3D).

The same area was imaged by switching a tip potential to induce lactate IT and raster scanning a tip at the gap between the tip and bacteria,  $d = 0.51 \ \mu m \ (1.20 \ d/a)$  (Figure 3C). An initial current of ~30 pA above a glass substrate in the SECM image is nearly the same as  $i_{T,\infty}$  of lactate IT, and corresponds to ~0.26 mM of lactate, as determined by eq 1. As no exogenous lactate is added to the medium, this amount of lactate is produced by S. mitis, and diffuses into bulk solution near the immobilized bacteria. In this metabolite-mapping image, individual S. mitis and C. matruchotii were successfully resolved with respect to both morphological and functional differences. Specifically, high tip currents of 50 pA corresponding to 167% of  $i_{T,\infty}$  are obtained over a single spherical object, whereas dramatically low tip currents of ~14 pA, i.e., 47% of  $i_{T,\infty}$  are obtained over a long filamentous feature in contact with a spherical one, and tip currents reach 22-24 pA, i.e., 75-80% of  $i_{T,\infty}$  above the rest of a filamentous object far apart from S. mitis (Figure 3C,E). These unique morphologies identified in the lactate-mapping SECM image are consistent with the shapes observed in optical microscopy, where spherical S. mitis surround a long filamentous C. matruchotii (similar to the optical microscopic image with white arrows for S. mitis and blue arrows for C. matruchotii shown in Figure 3A).

High tip currents above *S. mitis* are mainly due to the steady excretion of lactate as a fermentation product. By contrast, low tip currents above *C. matruchotii* are attributed to swift in situ

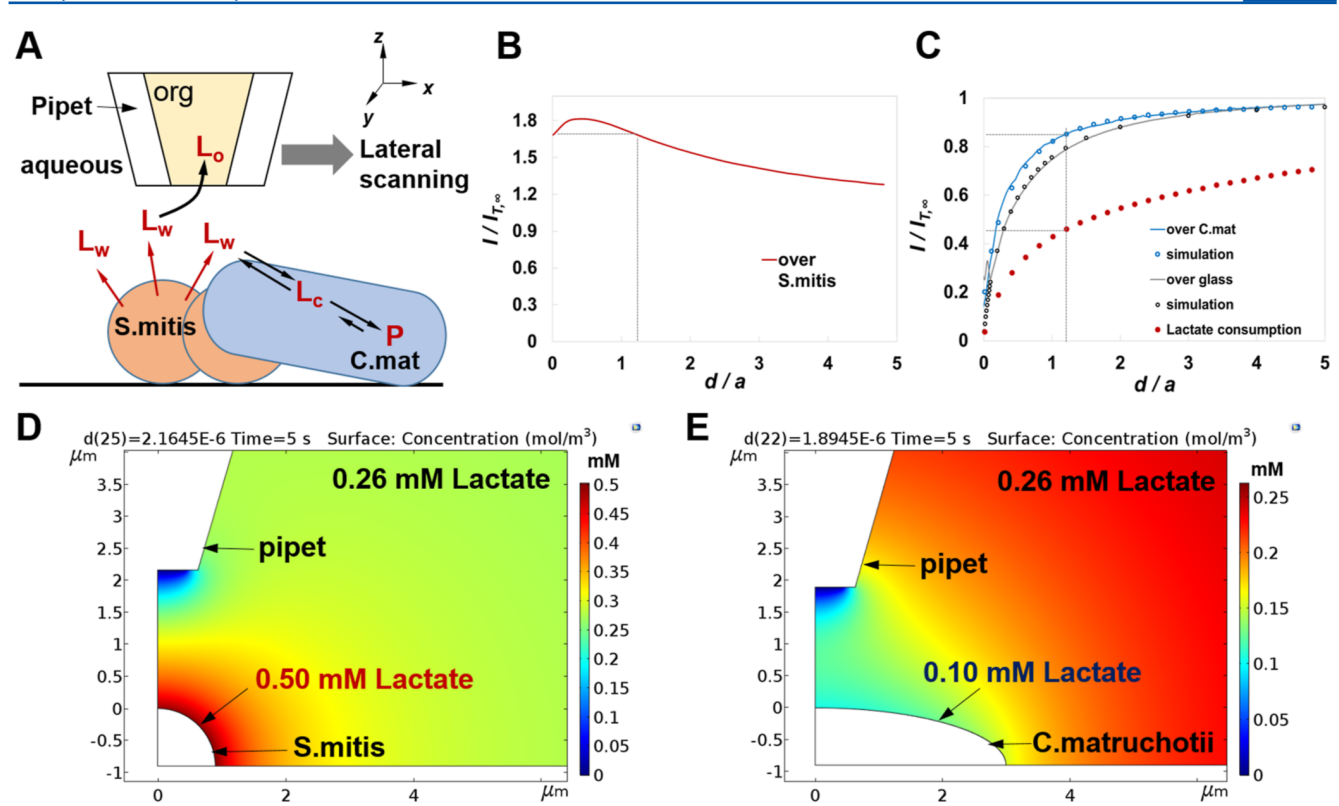


Figure 4. (A) Illustrated scheme of constant-height SECM imaging (lateral scanning along the x- and y-axis) over S. mitis and C. matruchotii coculture during in situ production and consumption of lactate, respectively. (B) Simulated SECM approach curve based on lactate IT over S. mitis producing lactate at a rate of  $2.7 \pm 0.1 \times 10^{-4}$  cm/s considering the determined BM permeability,  $k_1 = 2.4 \pm 0.1 \times 10^{-4}$  cm/s. (C) Theoretically simulated SECM approach curve based on lactate IT over a C. matruchotii consuming lactate at a rate of  $k_{c,f} \ge 5 \times 10^6$  s<sup>-1</sup> (closed red circles), compared with SECM approach curves over C. matruchotii determined by BM permeability ( $k_1 = 2.4 \pm 0.1 \times 10^{-4} \pm 0$ 

consumption of lactate by C. matruchotii as well as the hindered diffusional flux of lactate to the tip by the BM of C. matruchotii. If the tip current over C. matruchotii is only governed by inherent BM permeability to lactate, the resulting tip current at the gap of 1.20 d/a between the tip and a bacterium would be ~80% of  $i_{T,\infty}$ , i.e., ~24 pA, as obtained in the SECM approach curve (Figure 2A). In fact, 22-24 pA along a filamentous C. matruchotii far apart from S. mitis was observed, which is close to the tip currents determined by BM permeability. However, ~14 pA current above C. matruchotii contacting with S. mitis (red circle in Figure 3E) is much lower than the tip current expected from SECM approach curves in Figure 2A. Interestingly, this lower tip current is not due to the taller height of the bacterium, thus a smaller gap between the tip and the bacterium. It is confirmed by monotonic decreases in tip currents along the scanning axis and time in topographical SECM image and chronoamperometric responses (Figure 3B,D), respectively, indicating no apparent protrusion on C. matruchotii in close proximity to S. mitis. Accordingly, the lower tip current results from local depletion of lactate by C. matruchotii via lactate catabolism. Non-uniform consumption of lactate along the length of C. matruchotii can be related to proximity with S. mitis. As a result, the dramatic contrast of tip currents above two different species in the lactate-mapping SECM image visually confirms the real-time chemical exchange between S. mitis and C. matruchotii through simultaneous lactate production and its consumption,

respectively. Each monoculture was separately studied by SECM to confirm that lactate is only produced by *S. mitis* and not by *C. matruchotii* (see the Supporting Information). Noteworthily, this is the first successful case of real-time visualization of in situ metabolic interactions between two abundant oral bacterial species at a single-cell level, with insights into their commensal relationship, which cannot be elucidated by optical microscopic imaging.

Earlier, the Koley group studied the real-time metabolic interactions between dual species biofilms of lactate-producing *Streptococcus mutans* and H<sub>2</sub>O<sub>2</sub>-producing *Streptococcus gordonii* by constructing a pH profile by utilizing a carbon-based potentiometric pH microsensor as an SECM probe.<sup>17</sup> While a pH microsensor responds to lactate produced by *S. mutans*,<sup>17</sup> it cannot differentiate various acidic end products, e.g., formate, lactate, and acetate.<sup>30</sup> Also, the logarithmic dependence of potential response on the acidic product concentration limits sensitivity in local metabolite measurements.<sup>31–33</sup> Contrarily, our pipet tip amperometrically senses pristine lactate by selectively inducing lactate ITs, where the resulting current is directly proportional to local lactate concentration,<sup>31–33</sup> thereby enabling highly sensitive measurements in this single-cell study.

Quantitative Assessment of Mechanistic Interactions between Individual Commensal Bacteria by Finite Element Simulation. The commensal relationship between two strains is quantitatively assessed at a single-cell level using finite element simulation (details in the Supporting Information). In this simulation, lactate produced by *S. mitis* is released to aqueous bulk solution at a rate determined by the inherent BM permeability for efflux (eq 4), and diffuses near *C. matruchotii*, which readily oxidizes it (eq 5), while a tip senses local lactate in aqueous solution by inducing lactate IT under diffusion-limited conditions (eq 6) as shown below.

(S. 
$$mitis$$
) $L_{S.mitis}$  (bacteria)  $\stackrel{k_2}{\rightleftharpoons} L_w$  (aq, outer solution) (4)

(C. matruchotii) L<sub>w</sub> (aq, outer solution)

$$\begin{array}{c} \overset{k_{1}}{\rightleftarrows} \ L_{C} \ (\text{bacteria}) \\ \overset{k_{c,f}}{\rightleftarrows} \ P \ (\text{bacteria}) \\ \overset{k_{c,b}}{\rightleftarrows} \ P \ (\text{bacteria}) \end{array} \label{eq:controller}$$

$$(pipet)L_w(aq, outer solution) \rightleftharpoons L_o(org)$$
 (6)

where  $L_{S.mitis}$  is a lactate inside S. mitis,  $L_w$  is a lactate in outer aqueous solution,  $L_c$  is a lactate permeated in C. matruchotii,  $L_o$ is a lactate in the internal organic solution of a pipet tip, and P is a product of lactate oxidation.  $k_2$  and  $k_1$  are the first-order heterogeneous rate constants of forward and backward reactions, respectively, as shown in eq 4, where  $k_1$  and  $k_2$  are the same values determined in eq 3, i.e.,  $k_1 = 2.4 (\pm 0.1) \times 10^{-4}$ cm/s and  $k_2 = k_1/K_e$ . The partitioning equilibrium constant of lactate between in the bacteria and the outer solution, i.e.,  $c_2^0/c_1^0$  $(= k_1/k_2)$ , is considered equivalently to the partitioning equilibrium constant,  $K_e$  of small probe ions, TEA<sup>+</sup>, in eq 3, thereby being  $\sim 0.9$  for the monovalent ion. Also,  $k_1$  and  $k_2$ are the first-order heterogeneous rate constants of forward and backward reactions, respectively in eq 5, where the  $k_1$  value is as the same as that of BM permeability, i.e.,  $2.4 (\pm 0.1) \times 10^{-4}$ cm/s, as determined in eq 3. Further,  $k_{c,f}$  and  $k_{c,b}$  are the firstorder homogeneous rate constants of forward and backward reactions, as shown in eq 5, i.e., the oxidation of permeated lactate by C. matruchotii. Assuming a constant concentration of lactate dehydrogenase in C. matruchotii, a pseudo first-order homogeneous reaction is considered for lactate oxidation, as shown in eq 5.

A two-phase SECM diffusion problem was defined and solved in a 2D cylindrical model, where a tip was located above the center of a single bacterium of S. mitis or C. matruchotii (Figure 4D or 4E, respectively), and theoretical curves based on lactate IT were obtained (Figure 4B,C, see the Supporting Information). In this work, the BMs of both bacteria were treated as laterally homogeneous membranes with unique permeability,  $k_1$  determined by eq 2. Herein, the amperometric current response above the bacteria is a function of the tipbacteria distance and permeability as well as the concentration of lactate. First, a theoretical approach curve over S. mitis producing lactate is simulated, where steadily produced lactates are released at a rate of  $k_2$  (=  $k_1/K_e$  in eq 3), 2.7 ( $\pm 0.1$ )  $\times$  10<sup>-4</sup> cm/s from S. mitis in the presence of 0.26 mM lactate in aqueous bulk solution (Figure 4B). In this theoretical curve,  $\sim$ 1.67-fold increase in tip currents from  $i_{T,\infty}$  is obtained at 1.2 d/a, i.e., at the gap between the tip and bacteria,  $d = 0.51 \ \mu m$ . Notably, this increased current above S. mitis is consistent with the enhanced currents above S. mitis in a lactate-mapping SECM image (Figure 3C,E). The resulting concentration profile of lactate near *S. mitis* and a tip is depicted in Figure 4D, where the lactate concentration right above a single S. mitis is

estimated as 0.5 mM. This concentration, notably, is similar to the lactate concentration of saliva in healthy humans with a range within 3.5 mM.<sup>34</sup>

Another theoretical curve over C. matruchotii is simulated, where lactate diffusing from adjacent S. mitis permeates the C. matruchotii BM, and is readily oxidized by C. matruchotii. In this case, the rapid consumption of lactate appreciably decreases the lactate concentration near C. matruchotii, thus resulting in much smaller tip currents than currents only governed by BM permeability without lactate consumption (Figure 4C, red closed circles and blue open circles, respectively). Under this condition,  $\sim$ 47% of  $i_{T,\infty}$  can be theoretically predicted at 1.2 d/a, while  $\sim 83\%$  of  $i_{T,\infty}$  is anticipated if no lactate consumption occurs by C. matruchotii. In fact, SECM image and chronoamperometric responses, as shown in Figure 3C,E, yielded tip currents of ~14 pA at the gap and  $d = 0.51 \mu m$  between the tip and C. matruchotii adjacent to *S. mitis*, which is ~47% of  $i_{T,\infty}$  (~30 pA), as predicted in this theoretical simulation. This good agreement between the theoretical prediction and experimental currents validates the lactate consumption rate of *C. matruchotii* as  $k_{c,f} \ge$  $5 \times 10^6 \, \mathrm{s^{-1}}$  with thermodynamically favorable lactate oxidation under aerobic conditions, <sup>13,35</sup> i.e., an equilibrium constant,  $K_{\mathrm{eq}}$ =  $k_{\rm c,f}/k_{\rm c,b} \ge 10^{20}$  assumed in the theoretical simulation (eq 5). The simulated concentration profile of lactate near C. matruchotii and a pipet tip is depicted in Figure 4E, where the lactate concentration right above a single C. matruchotii is estimated as 0.1 mM. Noticeably, the determined  $k_{c,f}$  value is in a reasonable range considering the theoretical association constant of lactate substrate and lactate dehydrogenase based on the diffusion limit estimated by 36

$$k_{\rm a,d} = 4\pi N_{\rm A} (D_{\rm E} + D_{\rm L}) d \tag{7}$$

where  $N_{\rm A}$  is Avogadro's number,  $d=1.5\times 10^{-7}$  cm is the enzyme–substrate separation at their collision, and  $D_{\rm L}$  and  $D_{\rm E}=\sim 5\times 10^{-6}$  cm²/s are diffusion coefficients of lactate and free enzyme in the cell. In our given system,  $k_{\rm a,d}=\sim 1.1\times 10^{10}$  M $^{-1}$  s $^{-1}$  can be estimated, which results in the diffusion-limited  $k_{\rm c,f}$  value of  $\sim 6.6\times 10^6$  s $^{-1}$  with a steady concentration of  $\sim 707$  mU/mL (i.e.,  $\sim 0.6$  mM for 1 h) lactate dehydrogenase produced by bacteria.

In Figure 3C,E, tip currents above C. matruchotii far from S. mitis reach 22-24 pA of ~80% of  $i_{T,\infty}$ , which corresponds to currents in theoretical curves governed by intrinsic BM permeability (blue open circles in Figure 4C). This result clearly indicates negligible oxidation of lactate by C. matruchotii far from the source of lactate supply. Remarkably, the high spatial resolution of SECM measurements reveals a nonuniform efficiency of lactate oxidation along the length of the filamentous C. matruchotii cell. More efficient depletion of local lactate is facilitated by lactate oxidation of C. matruchotii adjacent to S. mitis when producing lactate, which can be a key mechanism supporting the previously described "corncob" spatial arrangement between these species in vivo under aerobic conditions.<sup>9,10</sup> As a result, the in situ metabolic interactions between two oral bacteria in close proximity explain the fitness benefit provided by C. matruchotii to S. mitis, 13 helping preserve their relationship in the oral cavity.

Significantly, we emphasize that real-time study of SECM imaging enabled us to unequivocally demonstrate in situ the metabolic cooperation between individual bacteria via concurrent lactate production and consumption at a single-cell level for the first time and quantitatively reveal their

mechanistic relationship. Traditional approaches to study interactions in polymicrobial communities are typically based on microscopy observations as well as genomics-based approaches (RNASeq, etc.).<sup>38,39</sup> Although powerful, these methods can only generate hypotheses regarding biochemical mechanisms of interaction. Biochemical studies employed for further investigation have been suitable for testing large-scale populations but do not fully mimic the intimate cell-cell interactions observed in in vivo biofilm structures. In that sense, our successful application of SECM toward polymicrobial interactions opens up a new route to investigate multispecies cooperation and competition via real-time probing of metabolites in situ and provides a new diagnostic tool to determine whether changes in the oral microbiome precede clinical signs of disease, thus enabling the use of the oral microbiome in the prediction of future disease risk.

## CONCLUSIONS

We applied nanoscale SECM with submicropipet-supported ITIES probes to not only image the permeability of BMs but also visualize the chemical communication between two highly abundant species, S. mitis and C. matruchotii in SUPP at singlecell resolution in real time. The results from the SECM experiments revealed their commensal relationship via metabolic synergy, which cannot be observed by either optical imaging or other conventional assays. Specifically, permeability imaging by SECM verified that the Gram-positive BM is 2 orders of magnitude less permeable to small probe ions, TEA+, than to eukaryotic membranes. The electrochemical mapping of lactate by SECM near S. mitis and C. matruchotii coculture enabled us to probe the local concentration of lactate produced by S. mitis and simultaneously oxidized by C. matruchotii in situ, thereby visually confirming previously hypothesized metabolite exchange 13 at the single-cell level and supporting their observed in vivo spatial organization. Using finite element analysis, the mechanistic interaction between coculture was quantitatively assessed at the single-cell level as well. Considering the role of lactate as an immunomodulatory molecule as well as a microbial metabolic product, our unique approach to real-time monitor local lactate between oral commensal bacteria and the quantitative assessment of their metabolic communication can provide a new diagnostic methodology to evaluate human health status and future disease risk.

# ASSOCIATED CONTENT

# **Solution** Supporting Information

The Supporting Information is available free of charge at https://pubs.acs.org/doi/10.1021/acs.analchem.3c01498.

Supplemental methods, optical microscopic image of coculture bacterial sample, SECM imaging of S. mitis monoculture, SECM imaging of C. matruchotii monoculture, and finite element simulation by COMSOL multiphysics (PDF)

Detailed COMSOL model reports for bacterial membrane permeability (PDF)

## AUTHOR INFORMATION

#### **Corresponding Author**

Jiyeon Kim - Department of Chemistry, The University of Rhode Island, Kingston, Rhode Island 02881, United States;

orcid.org/0000-0002-7624-6766; Phone: +1 (401) 874-2143; Email: jkim25@uri.edu

#### **Authors**

pubs.acs.org/ac

Surendra R. Puri – Department of Chemistry, The University of Rhode Island, Kingston, Rhode Island 02881, United States

Eric Almeida - Department of Cell and Molecular Biology, The University of Rhode Island, Kingston, Rhode Island 02881, United States

Subhashini Elangovan - Department of Chemistry, The University of Rhode Island, Kingston, Rhode Island 02881, United States

Alex Labossiere – Department of Cell and Molecular Biology, The University of Rhode Island, Kingston, Rhode Island 02881, United States

Cybele Collins - Department of Cell and Molecular Biology, The University of Rhode Island, Kingston, Rhode Island 02881, United States

Matthew Ramsey - Department of Cell and Molecular Biology, The University of Rhode Island, Kingston, Rhode Island 02881, United States

Complete contact information is available at: https://pubs.acs.org/10.1021/acs.analchem.3c01498

#### **Author Contributions**

S.P. and E.A. contributed to this work equally. S.E. has contributed to the initial draft preparation but has been unreachable and did not participate in the peer review of this manuscript.

#### **Notes**

The authors declare no competing financial interest.

# ACKNOWLEDGMENTS

This work was supported by the NSF Career (CHE-2046363—J.K.), Medical Research Fund (20174373—J.K.) from Rhode Island Foundation, the Rhode Island Institutional Development Award (IDeA), the NIGMS/RI-INBRE early career development award (P20GM103430-J.K. and P20GM103430-M.R.), the NIDCR/NIH(R01DE027958-M.R.), and the USDA National Institute of Food and Agriculture, Hatch Formula project accession number 1017848 (M.R.).

#### REFERENCES

- (1) Lee, Y.-H.; Chung, S. W.; Auh, Q.-S.; Hong, S.-J.; Lee, Y.-A.; Jung, J.; Lee, G.-J.; Park, H. J.; Shin, S.-I.; Hong, J.-Y. Diagnostics 2021, 11, 1283.
- (2) Dewhirst, F. E.; Chen, T.; Izard, J.; Paster, B. J.; Tanner, A. C.; Yu, W. H.; Lakshmanan, A.; Wade, W. G. J. Bacteriol. 2010, 192, 5002-5017.
- (3) Gao, L.; Xu, T.; Huang, G.; Jiang, S.; Gu, Y.; Chen, F. Protein Cell 2018, 9, 488-500.
- (4) Bourgeois, D.; Inquimbert, C.; Ottolenghi, L.; Carrouel, F. Microorganisms 2019, 7, 424.
- (5) Radaic, A.; Kapila, Y. L. Comput. Struct. Biotechnol. J. 2021, 19, 1335-1360.
- (6) Peng, X.; Cheng, L.; You, Y.; Tang, C.; Ren, B.; Li, Y.; Xu, X.; Zhou, X. Int. J. Oral Sci. 2022, 14, 14.
- (7) Xiao, C.; Ran, S.; Huang, Z.; Liang, J. Front. Microbiol. 2016, 7,
- (8) Schoilew, K.; Ueffing, H.; Dalpke, A.; Wolff, B.; Frese, C.; Wolff, D.; Boutin, S. J. Oral Microbiol. 2019, 11, 1633194.

- (9) Mark Welch, J. L.; Rossetti, B. J.; Reijebm, C. W.; Borisy, G. G. Proc. Natl. Acad. Sci. U.S.A. 2016, 113, E791–E800.
- (10) Morillo-Lopez, V.; Sjaarda, A.; Islam, I.; Borisy, G.; Mark Welch, J. L. *Microbiome* **2022**, *10*, 145.
- (11) Mashimo, P. A.; Yamamoto, Y.; Nakamura, M.; Reynolds, H. S.; Genco, R. J. *J. Periodontol.* **1985**, *56*, 548–552.
- (12) Redanz, S.; Cheng, X.; Giacaman, R. A.; Pfeifer, C. S.; Merritt, J.; Kreth, J. *Methods Mol. Biol.* **2018**, 33, 337–352.
- (13) Almeida, E.; Puri, S. R.; Elangovan, S.; Kim, J.; Ramsey, M. Bacterial Multispecies Interaction Mechanisms Dictate Biogeographical Arrangement between the Oral Commensals Corynebacterium Matruchotii and Streptococcus Mitis, 2023. manuscript submitted. (b) Almeida, E.; Puri, S. R.; Elangovan, S.; Kim, J.; Ramsey, M. bioRxiv 2022, DOI: 10.1101/2022.05.09.491233.
- (14) Connell, J. L.; Kim, J.; Shear, J. B.; Bard, A. J.; Whiteley, M. Proc. Natl. Acad. Sci. U.S.A. 2014, 111, 18255–18260.
- (15) Koley, D.; Ramsey, M. M.; Bard, A. J.; Whiteley, M. Proc. Natl. Acad. Sci. U.S.A. 2011, 108, 19996–20001.
- (16) Liu, X.; Ramsey, M. M.; Chen, X.; Koley, D.; Whiteley, M.; Bard, A. J. Proc. Natl. Acad. Sci. U.S.A. 2011, 108, 2668–2673.
- (17) Joshi, V. S.; Sheet, P. S.; Cullin, N.; Kreth, J.; Koley, D. Anal. Chem. 2017, 89, 11044–11052.
- (18) Zhan, D.; Li, X.; Zhan, W.; Fan, F. R. F.; Bard, A. J. Anal. Chem. **2007**, 79, 5225–5231.
- (19) Zhan, D.; Fan, F. R. F.; Bard, A. J. Proc. Natl. Acad. Sci. U.S.A. 2008, 105, 12118-12122.
- (20) Kim, J.; Renault, C.; Nioradze, N.; Arroyo-Curras, N.; Leonard, K. C.; Bard, A. J. *J. Am. Chem. Soc.* **2016**, *138*, 8560–8568.
- (21) Kim, J.; Renault, C.; Nioradze, N.; Arroyo-Curras, N.; Leonard, K. C.; Bard, A. J. Anal. Chem. **2016**, 88, 10284–10289.
- (22) Pathirathna, P.; Balla, R. J.; Jantz, D. T.; Kurapati, N.; Gramm, E. R.; Leonard, K. C.; Amemiya, S. *Anal. Chem.* **2019**, *91*, 5446–5454.
- (23) Mark Welch, J. L.; Rossetti, B. J.; Rieken, C. W.; Dewhirst, F. E.; Borisy, G. G. *Proc. Natl. Acad. Sci. U.S.A.* **2016**, *113*, E791–E800.
- (24) Puri, S. R.; Kim, J. Anal. Chem. 2019, 91, 1873-1879.
- (25) Chon, J.; Kim, M. Ther. Clin. Risk Manage. 2017, 13, 1439-
- (26) Forbes, B. A.; Sahm, D. F.; Weissfeld, A. S. Bailey and Scott's Diagnostic Microbiology, 10th ed.; C.V. Mosby Company: St. Louis, MO, 1998.
- (27) Guo, J.; Amemiya, S. Anal. Chem. 2005, 77, 2147-2156.
- (28) Nikaido, H. Microbiol. Mol. Biol. Rev. 2003, 67, 593-656.
- (29) Kim, J.; Izadyar, A.; Nioradze, N.; Amemiya, S. J. Am. Chem. Soc. 2013, 135, 2321–2329.
- (30) Baker, J. L.; Faustoferri, R. C.; Quivey, R. G., Jr Mol. Oral Microbiol. 2017, 32, 107-117.
- (31) Bakker, E.; Bühlmann, P.; Pretsch, E. Chem. Rev. 1997, 97, 3083-3132.
- (32) Amemiya, S. Potentiometric Ion-Selective Electrodes. In *Handbook of Electrochemistry*; Zoski, C. G., Ed.; Elsevier: New York, 2007, pp 261–294.
- (33) Henn, D.; Cammann, K. Electroanalysis 2000, 12, 1263-1271.
- (34) Spehar-Délèze, A.-M.; Anastasova, S.; Vadgama, P. Chemosensors 2021, 9, 195.
- (35) Iwami, Y.; Higuchi, M.; Yamada, T.; Araya, S. J. Dent. Res. 1972, 51, 1683.
- (36) Houston, P. L. Chemical Kinetics and Reactions Dynamics; Dover Publications, Inc.: New York, 2001.
- (37) Van den Bossche, S.; Vandeplassche, E.; Ostyn, L.; Coenye, T.; Crabbé, A. Front. Cell. Infect. Microbiol. 2020, 10, 494.
- (38) Peters, B. M.; Jabra-Rizk, M. A.; O'May, G. A.; Costerton, J. W.; Shirtliff, M. E. Clin. Microbiol. Rev. 2012, 25, 193–213.
- (39) Zhang, M.; Whiteley, M.; Lewin, G. R. mBio 2022, 13, No. e00235-22.